

Metropolis simulations of Met-Enkephalin with solvent-accessible area parameterizations

Bernd A. Berg

*Department of Physics, Florida State University, Tallahassee, FL 32306 and
School of Computational Science and Information Technology, Florida State University, Tallahassee, FL32306*

Hsiao-Ping Hsu

John-von-Neumann Institute for Computing, Forschungszentrum Jülich, D-52425 Jülich, Germany

(Dated: November 6, 2018)

We investigate the solvent-accessible area method by means of Metropolis simulations of the brain peptide Met-Enkephalin at 300 K. For the energy function ECEPP/2 nine atomic solvation parameter (ASP) sets are studied. The simulations are compared with one another, with simulations with a distance dependent electrostatic permittivity $\epsilon(r)$, and with vacuum simulations ($\epsilon = 2$). Parallel tempering and the biased Metropolis techniques RM₁ are employed and their performance is evaluated. The measured observables include energy and dihedral probability densities (pds), integrated autocorrelation times, and acceptance rates. Two of the ASP sets turn out to be unsuitable for these simulations. For all other systems selected configurations are minimized in search of the global energy minima, which are found for the vacuum and the $\epsilon(r)$ system, but for none of the ASP models. Other observables show a remarkable dependence on the ASPs. In particular, we find three ASP sets for which the autocorrelations at 300 K are considerably smaller than for vacuum simulations.

PACS numbers: 05.10.Ln, 87.16.-v, 87.14.Ee.

I. INTRODUCTION

In nature biomolecules exist in the environment of solvents, thus the molecule-solvent interactions must be taken into account. It is very computer time consuming to simulate models for which the molecules of the surrounding water are treated explicitly. Therefore, a number of approximations of solvent effects have been developed. In the solvent-accessible area approach [1, 2, 3] it is assumed that the protein-solvent interaction is given by the sum of the surface area of each atomic group times the atomic solvation parameter (ASP). The choice of a set of ASPs (also called hydrophobicity parameters or simply hydrophobicities) defines a model of solvation. However, there is no agreement on how to determine the universally best set of ASPs, or a at least the best set for some limited purpose. For instance, eight sets were reviewed and studied by Juffer et al. [4] and it was found that they give rather distinct contributions to the free energy of proteins folding.

In this paper we investigate how different ASP sets modify the Metropolis simulations of the small brain peptide Met-Enkephalin (Tyr-Gly-Gly-Phe-Met) at 300 K. The reason for the choice of Met-Enkephalin is that its vacuum properties define a reference system for testing numerical methods, e.g. [5, 6, 7, 8, 9, 10]. Therefore, Met-Enkephalin appears to be well suited to set references for the inclusion of solvent effects as well, but we are only aware of few articles [11, 12], which comment on the modifications due to including a solvent model.

We set our simulation temperature to 300 K, because room temperature is the physical temperature at which biological activity takes place. Most of the previous sim-

ulations of Met-Enkephalin in vacuum were performed at much lower temperatures or employed elaborate minimization techniques with the aim to determine the global energy minimum (GEM). Only recently [10] it was shown that the GEM is well accessible by local minimization of properly selected configurations from an equilibrium time series at 300 K. Precisely this should be the case for a GEM which is of relevance at physical temperatures.

For our simulations we use the program package SMMP [13] (Simple Molecular Mechanics for Proteins) together with parallel tempering [14, 15, 16] (PT) and the recently introduced [10] biased Metropolis technique RM₁ (rugged Metropolis – approximation 1). SMMP implements a number of all-atom energy functions, describing the intramolecular interactions, and nine ASP sets [3, 17, 18, 19, 20, 21, 22, 23] to model the molecule solvent interactions. We use the ECEPP/2 [24] (Empirical Conformational Energy Program for Peptides) energy function with fully variable ω angles and simulate all nine ASP sets. For comparison we simulate also Met-Enkephalin in vacuum and with the distance dependent electrostatic permittivity $\epsilon(r)$ of Ref. [25].

The paper is organized as follows: The energy functions and Metropolis methods used are explained in Sec. II. In Sec. III we present our results from simulations of the brain peptide Met-Enkephalin. Summary and conclusions are given in Sec. IV.

II. MODELS AND METHODS

A. ASP sets

In all-atom models of biomolecules the total conformational energy of the intramolecular interactions E_I is given as the sum of the electrostatic, the Lennard-Jones (Van der Waals), the hydrogen bond, and the torsional contributions,

$$E_I = 332 \sum_{i < j} \frac{q_i q_j}{\epsilon r_{ij}} + \sum_{i < j} \left(\frac{A_{ij}^{LJ}}{r_{ij}^{12}} - \frac{B_{ij}^{LJ}}{r_{ij}^6} \right) + \sum_{i < j} \left(\frac{A_{ij}^{HB}}{r_{ij}^{12}} - \frac{B_{ij}^{HB}}{r_{ij}^{10}} \right) + \sum_k U_k [1 \pm \cos(n_k \phi_k)]. \quad (1)$$

Here r_{ij} is the distance between atoms i and j , q_i and q_j are the partial charges on the atoms i and j , ϵ is the electric permittivity of the environment, A_{ij} , B_{ij} , C_{ij} and D_{ij} are parameters that define the well depth and width for a given Lennard-Jones or hydrogen bond interaction, and ϕ_k is the k th torsion angle. The units are as follows: distances are in Å, charges are in units of the electronic charge and energies are in kcal/mol.

One of the simplest ways to include interactions with water is to assume a distance dependent electrostatic permittivity according to the formula [25, 26]

$$\epsilon(r) = D - \frac{D-2}{2} [(sr)^2 + 2sr + 2] e^{-sr}. \quad (2)$$

Empirical values for the parameters D and s are chosen, so that for large distances the permittivity takes the value of bulk water, $\epsilon = 80$, and the value $\epsilon = 2$ for short distances, i.e. for the interior of the molecule. Approximating solvation effects in this way is implemented as an option in SMMP. It allows to include solvation effects without any significant slowing down over the vacuum simulation with $\epsilon = 2$. The approach is clearly an oversimplification, because atoms which are close to each other do not necessarily have to be simultaneously in the interior of the molecule. Reversely, two atoms which are separated by a large distance may still be in the interior of the molecule. More elaborated approaches are asked for.

If the molecule-solvent interaction is proportional to the surface area of the atomic groups, it is given by the sum of contributions of a product of the surface area of each atomic group and the atomic solvation parameter [3],

$$E_{\text{sol}} = \sum_i \sigma_i A_i. \quad (3)$$

Here E_{sol} is the solvation energy and the sum is over all atomic groups. A_i is the solvent accessible surface area and σ_i the atomic solvation parameter of group i . The choice of a set of ASPs σ_i defines a model of solvation. There are nine sets of ASPs in the SMMP package, which

TABLE I: Atomic solvation parameter sets implemented in SMMP. The first column gives the value of the SMMP parameter `itysol` and the second column the letter code used in SMMP. In the author column we give also the year of publication. The last column indicates the method used as explained in the text.

		Authors	
1	OONS	Ooi, Obatake, Nemethy, Scheraga [17] 1987	v/w
2	JRF	Vila, Williams, Vásquez, Scheraga [20] 1991	v/w
3	WE92	Wesson and Eisenberg [21] 1992	v/w
4	EM86	Eisenberg and McLachlan [3] 1986	o/w
5	SCH1	Eisenberg, Wesson, Yamashita [18] 1989	o/w
6	SCH2	Kim [19], see [4] 1990	o/w
7	SCH3	Wesson and Eisenberg [21] 1992	v/w
8	SCH4	Schiffer, Caldwell, Kollman, Stroud [22] 1993	v/ws
9	BM	Freyberg, Richmond, Brown [23] 1993	cla

we list in Table I. Columns one and two of this table gives the notations used in SMMP to identify the different sets.

Eisenberg and McLachlan [3] were the first to determine a set of ASPs (`itysol`= 4, EM86 in the SMMP notation). For this, they considered the process of transferring atoms or groups of atoms from the interior of a protein to aqueous solution and used transfer energies of amino acids from *n*-octanol to water as reported in [27]. The ASPs are then determined by least-square fitting. Octanol is chosen, because it apparently resembles the interior of a protein. With the exception of [22] and [23], the other authors used similar methods with the major variation that instead of transfer energies with respect to octanol-water (o/w) also transfer energies with respect to vacuum-water (v/w) were used (for early determination of v/w transfer energies see [28, 29]). The last column of Table I indicates whether the transfer energy is o/w or v/w. In the chronological order [3, 18, 21] Eisenberg and collaborators contributed the parameter sets EM86, SCH1, WE92 and SCH3. Scheraga and collaborators [17, 20] contributed the parameter sets OONS and JRF. Here it should be noted that some of the original ASP sets were modified in course of time. For `itysol`= 1, ..., 8 SMMP implements the parameters as reviewed and tabulated in Ref. [4], where in turn the sets SCH1 to SCH4 are simply taken from Schiffer et al.[22]. Table 1 of SMMP [13] lists the implemented ASPs for `itysol` = 1, ..., 8.

Somewhat special cases are the ASP sets SCH4 [22] and BM [23]. SCH4 was determined by comparison of the crystal structure from molecular dynamics simulations of small peptides and proteins in explicit water with similar simulations using an ASP solvation term (v/ws). The BM set of SMMP relies on a specific classification (cla) of atomic groups, where for all non-hydrogen atoms the solvation coefficients are set to 1 kcal/mol per Å².

B. Metropolis methods

For the updating of our systems we use PT with two processors, one running at 300 K and the other at 400 K. This builds on the experience [10] with vacuum simulations of Met-Enkephalin for which the following observations are made:

1. The integrated autocorrelation time τ_{int} (defined below in this section) increases from 400 K to 300 K by a factor of ten for the (internal) energy and by factors of more than twenty for certain dihedral angles.
2. The energy probability densities (pds) at 300 K and 400 K overlap sufficiently, so that the PT method works, leading to an improvement factor of about 2.5 in the real time needed for the simulation (see Table I of Ref. [10]).

A brief description of the PT algorithm is given in the following. PT performs n canonical MC simulations at different β -values with Boltzmann weight factors

$$w_{B,i}(E^{(k)}) = e^{-\beta_i E_i^{(k)}} = e^{-H}, i = 0, \dots, n-1 \quad (4)$$

where $\beta_0 < \beta_1 < \dots < \beta_{n-2} < \beta_{n-1}$ and a configuration is denoted by k . PT allows the exchange of neighboring β -values

$$\beta_{i-1} \leftrightarrow \beta_i \text{ for } i = 1, \dots, n-1. \quad (5)$$

These transitions lead to the change

$$\begin{aligned} -\Delta H &= -\beta_{i-1} (E_i^{(k)} - E_{i-1}^{(k')}) - \beta_i (E_{i-1}^{(k')} - E_i^{(k)}) \\ &= (\beta_i - \beta_{i-1}) (E_i^{(k)} - E_{i-1}^{(k')}) \end{aligned} \quad (6)$$

which is accepted or rejected according to the Metropolis algorithm, i.e. with probability one for $\Delta H \leq 0$ and with probability $\exp(-\Delta H)$ for $\Delta H > 0$.

For the vacuum system the performance of the PT simulation was improved by an additional factor of two in Ref.[10] by using a first approximation, called RM₁, to the rugged Metropolis scheme introduced there. A (short) simulation at 400 K was used to obtain estimates $\bar{p}_j(v_j)$, $j = 1, \dots, 24$ of the pds of the 24 dihedral angles, which were then fed into the simulation. For a configuration change $k \rightarrow k'$ at temperature T_i the new configuration accepted with the probability

$$p_{\text{acpt}} = \min \left[1, \frac{\exp(-\beta_i E_i^{(k')}) \prod_{j=1}^{24} \bar{p}_j(v_j^{(k')})}{\exp(-\beta_i E_i^{(k)}) \prod_{j=1}^{24} \bar{p}_j(v_j^{(k)})} \right] \quad (7)$$

in the RM₁ updating scheme. In the present paper we report the improvement due to this biased updating for some of the ASP sets.

In the vacuum simulation it is possible to determine the GEM by minimizing selected configurations of the

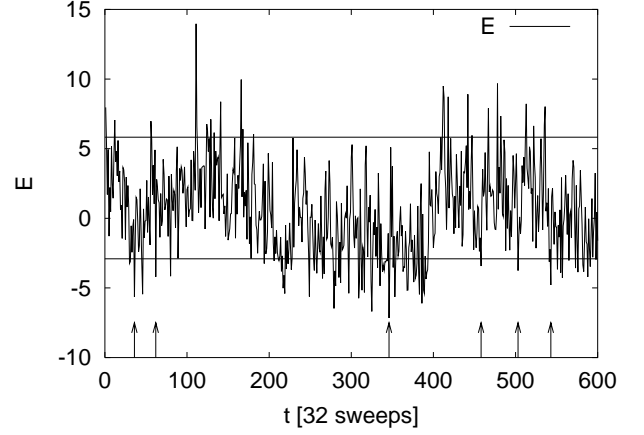


FIG. 1: Selection of configurations for local minimization from the energy time series at 300 K. The lower and upper straight lines indicate the quantiles $E_{0.1}$ and $E_{0.9}$, respectively.

300 K time series. Here we apply the same procedure to our PT simulation of the ASP sets introduced in the previous subsection:

1. We determine the lower 10% quantile $E_{0.1}$ and the upper 10% quantile $E_{0.9}$ of the energy distribution of our time series. This is done by sorting all energies in increasing order and finding the values which cut out the lower and upper 10% of the data. For the statistical concepts see, e.g., Ref. [30].
2. We partition the time series into bunches of configurations. A bunch contains the configurations from one crossing of the upper quantile $E_{0.9}$ to the next so that at least one crossing of the lower quantile $E_{0.1}$ is located between the two crossings of $E_{0.9}$. For each bunch we pick then its configuration of lowest energy. The idea behind this procedure is to pick minima of the time series, which are to a large degree statistically independent. In Fig. 1 the arrows indicate the energy values picked in that way from the first 600 configurations recorded in the RM₁ simulation of Ref. [10].
3. We run a conjugate gradient minimizer on all the selected configurations and thus obtain a set of configurations which are local energy minima. For the vacuum simulation [10] about 5% to 6% of the thus minimized configurations agree with the GEM.

To determine the speed at which the systems equilibrate, we measure the integrated autocorrelation time τ_{int} for the energy and each dihedral angle. In particular the integrated autocorrelation times are directly proportional to the computer run times needed to achieve the same statistical accuracy for each system. They thus determine the relative performance of distinct algorithms. For an observable f the autocorrelations are

$$C(t) = \langle f_0 f_t \rangle - \langle f \rangle^2 \quad (8)$$

where t labels the computer time. Defining $c(t) = C(t)/C(0)$, the time-dependent integrated autocorrelation time is given by

$$\tau_{\text{int}}(t) = 1 + 2 \sum_{t'=1}^t c(t'). \quad (9)$$

Formally the integrated autocorrelation time τ_{int} is defined by $\tau_{\text{int}} = \lim_{t \rightarrow \infty} \tau_{\text{int}}(t)$. Numerically, however, this limit cannot be reached as the noise of the estimator increases faster than the signal. Nevertheless, one can calculate reliable estimates by reaching a window of t values for which $\tau_{\text{int}}(t)$ becomes flat, while its error bars are still reasonably small. This is the method we employ in the next section, see Ref. [31] for a more detailed discussion of the integrated autocorrelation time.

III. RESULTS

A. Autocorrelations

The PT simulations with temperatures $T_0 = 400$ K and $T_1 = 300$ K are performed on the system in vacuum ($\epsilon = 2$), with $\epsilon(r)$ given by Eq. (2) and for the nine ASP sets of Table I. The dihedral angles updated in our simulations are fully variable in the range from $-\pi$ to π . We keep a time series of $2^{16} = 65536$ configurations for each replica (i.e., each of the two processor), in which subsequent configurations are separated by 32 sweeps. A sweep is defined by updating each dihedral angle once sequentially. Before starting with measurements $2^{18} = 262144$ sweeps are performed for reaching equilibrium. Thus, the entire simulation at one temperature relies on $2^{21} + 2^{18} = 2,359,296$ sweeps. On the Cray T3E, this takes about 14 hours for the vacuum system and 5×14 hours for each ASP set.

Results of the average energy, acceptance rates and integrated autocorrelations times for the energy E variable are shown in Table II. For the vacuum simulations and the ASP sets OONS and EM86 the time-dependent integrated autocorrelations times (9) are shown in Fig. 2. In each case a window of t values is reached for which $\tau_{\text{int}}(t)$ does no longer increase within its statistical errors. In the case of the vacuum simulations it even does decrease, but this is not significant due to the statistical error. These windows are then used to estimate the asymptotic τ_{int} values of Table II. With the exception of the ASP sets JRF and BM, the integrated autocorrelations times of all other sets are determined in the same way.

From Table II we see that the acceptance rates of the solvent models JRF and BM are much lower than for the other models. In essence the simulations of these two models get stuck, which implies that their integrated autocorrelation times cannot be measured. This is illustrated in Fig. 3 for the time-dependent integrated autocorrelation time of the energy at 300 K. The function $\tau_{\text{int}}(t)$ increases rapidly until it gets lost in the noise. The

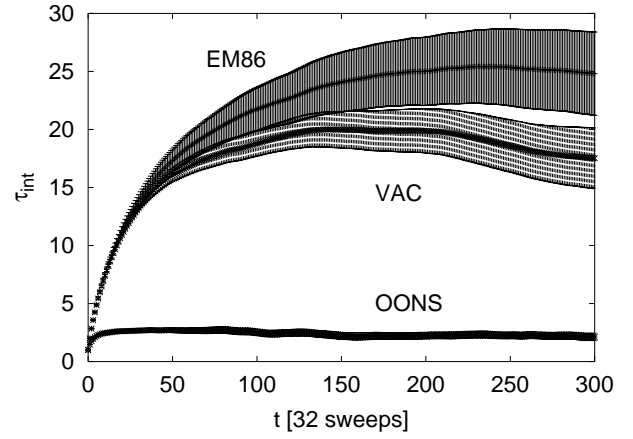


FIG. 2: The time-dependent integrated autocorrelation time for the energy at 300 K from our simulations of the vacuum system and two of the solvent models of Table I.

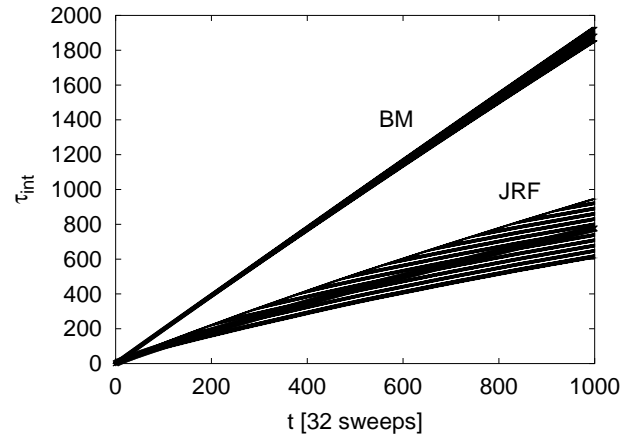


FIG. 3: The time-dependent integrated autocorrelation time for the energy at 300 K from our simulations of the solvent models JRF and BM.

pds of the dihedral angles of these two models are also erratic and the conclusion is that they cannot be used to describe Met-Enkephalin in solvent.

The energy couples to all dihedral angles and its integrated autocorrelation time is characteristic for the entire system, while the integrated autocorrelation times of the single dihedral angles vary heavily from angle to angle. For all our systems, but JRF and BM, we show in Fig. 4 the integrated autocorrelation times at 300 K for the energy and all dihedral angles. The notation v_i , $i = 0, 1, \dots, 24$ is used, where v_0 stands in for the energy E and for $i = 1, \dots, 24$ the v_i are the dihedral angles as used in the SMMP computer program. The relationship of the v_i angles to the conventional notation for dihedral angles and their residues is summarized in Table III, where it should be noted that the SMMP

TABLE II: Average energies $\langle E \rangle$ (Kcal/mol), acceptance rates and integrated autocorrelations times τ_{int} for the energy are shown for simulations in vacuum (VAC), with $\epsilon(r)$ of Eq. (2) and with the nine ASP introduced in Table I.

Set	$T = 400$ K			$T = 300$ K		
	$\langle E \rangle$	acpt	τ_{int}	$\langle E \rangle$	acpt	τ_{int}
VAC	7.07(03)	0.167	3.67(20)	1.29(06)	0.119	19.9(1.6)
$\epsilon(r)$	-12.00(03)	0.171	2.92(10)	-17.61(06)	0.121	14.35(75)
OONS	-13.80(01)	0.195	1.25(02)	-17.70(02)	0.143	2.64(14)
JRF	-311.69(44)	0.058	-	-319.08(40)	0.046	-
WE92	-15.76(02)	0.199	1.30(03)	-19.75(02)	0.145	2.94(07)
EM86	13.49(03)	0.158	4.71(21)	8.03(06)	0.116	25.0(2.9)
SCH1	10.45(03)	0.165	3.72(22)	4.95(06)	0.119	23.2(2.2)
SCH2	-18.33(02)	0.212	1.11(01)	-21.83(01)	0.160	1.89(05)
SCH3	13.33(03)	0.151	4.59(34)	8.33(06)	0.112	26.4(3.3)
SCH4	13.38(03)	0.158	4.35(17)	7.85(05)	0.115	25.1(2.1)
BM	630.4(3.9)	0.043	-	610.6(3.0)	0.037	-

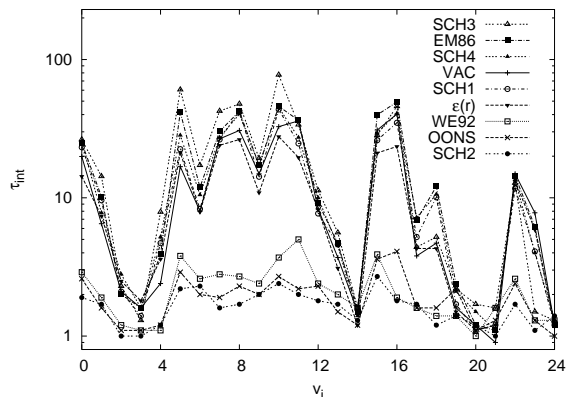


FIG. 4: Integrated autocorrelation times for the energies ($v_0 = E$) and the dihedral angles v_i , $i = 1, \dots, 24$ at $T=300$ K. The up-to-down order of the curves agrees at $i = 10$ with the order in the figure legend.

notation [13] differs from other literature [5, 8].

In Fig. 4 we see that for each dihedral angle v_i the integrated autocorrelation times $\tau_{\text{int}}[v_i]$ for the three solvent models OONS, WE92 and SCH2 are smaller than for the remaining systems, including the vacuum system. For the integrated autocorrelation time of the energy $\tau_{\text{int}}[E]$ this observation is already obvious from Table II. In particular, this means that the OONS, WE92 and SCH2 models require far less statistics than the vacuum run for achieving the same accuracy of results. Using the $\tau_{\text{int}}[E]$ results of Table II, we find a factor in the range 7 to 10, which more than offsets the factor of 5 by which the ASP model simulations are slower than the vacuum simulation. In the following the solvation models OONS, WE92 and SCH2 define the “fast class”, while the other models shown in Fig. 4 constitute the “slow class” (the models JRF and BM are omitted from this classification). “Good” behavior of the models OONS and WE92

has been previously observed [32].

The autocorrelation times in the fast class are so small that the resolution of 32 sweeps in our recorded time series becomes too crude. Namely, autocorrelations over less than 32 sweeps are then not measured and the integrated autocorrelation time approaches one as soon as autocorrelations stay within the range of 32 sweeps. To investigate this point further, we performed for the OONS, WE92 and SCH2 models simulations for which the configurations were recorded every four sweeps and the total statistics was reduced by the factor 1/8. In the new units of four sweeps the integrated autocorrelation time is larger by a factor which is bounded by $8 = 32/4$. The bound is assumed, if there is no improvement due to integrating additional small fluctuations out (i.e. due to the additional configuration in between the 32 sweeps, which are now kept in the time series).

For WE92 we report in the PT column of Table III the integrated autocorrelation times from the simulation with reduced statistics. For many dihedral angles the increase lies well below the factor of eight, showing that we gain in accuracy by averaging over small fluctuation within the range of 32 sweeps. On the other hand, nothing is gained by this extra averaging for several angles with large autocorrelations. In those case the simulations yield within their statistical errors the upper bound 8.

To supplement the vacuum results of Ref. [10], we repeated the WE92 PT simulations by using estimates of the dihedral pds from 400 K as input for the biased updating of Eq. (7). These results are reported in the PT-RM₁ column of Table III. As in the case of the vacuum simulations, we find an improvement of the PT performance by a factor of approximately two, which is also obtained for the other models of the fast class. For the slow class we checked by direct improvement of the original simulations on the ASP models EM86 and SCH4 and find again an acceleration by a factor of about two when we are using RM₁ updating.

TABLE III: Definitions of the dihedral angles together with their integrated autocorrelation times τ_{int} at 300 K for simulations of WE92 with a statistics reduced by 1/8 and configurations recorded every four sweeps. PT denotes the 400 K–300 K parallel tempering simulation. For PT-RM₁ the PT simulation is supplemented by the RM₁ biased updating (7) with input pds from 400 K. The factor of the last column denotes the increase of the PT τ_{int} over its values for the full WE92 simulations where configurations were recorded every 32 sweeps (8 is the upper bound for this factor).

var	angle	res [5, 8]	res [13]	PT-RM ₁	PT	factor
v_1	χ^1	Tyr-1	Tyr-1	6.9 (1.1)	11.6 (1.6)	6.1 (0.9)
v_2	χ^2	Tyr-1	Tyr-1	2.0 (0.2)	3.1 (0.5)	2.7 (0.5)
v_3	χ^6	Tyr-1	Tyr-1	1.0 (0.1)	1.3 (0.2)	1.3 (0.2)
v_4	ϕ	Tyr-1	Tyr-1	2.1 (0.2)	2.6 (0.4)	2.4 (0.4)
v_5	ψ	Tyr-1	Gly-2	12.6 (1.7)	15.7 (2.2)	4.1 (0.7)
v_6	ω	Tyr-1	Gly-2	3.9 (0.4)	14.4 (1.2)	5.6 (0.5)
v_7	ϕ	Gly-2	Gly-2	9.1 (1.0)	13.0 (1.4)	4.6 (0.6)
v_8	ψ	Gly-2	Gly-3	10.6 (1.3)	20.4 (3.1)	7.6 (1.2)
v_9	ω	Gly-2	Gly-3	3.4 (0.2)	16.0 (1.8)	6.7 (0.8)
v_{10}	ϕ	Gly-3	Gly-3	18.2 (3.2)	31.0 (5.1)	8.4 (1.5)
v_{11}	ψ	Gly-3	Phe-4	15.6 (2.9)	52 (13)	12 (4)
v_{12}	ω	Gly-3	Phe-4	4.4 (0.6)	17.7 (2.7)	7.7 (1.3)
v_{13}	χ^1	Phe-4	Phe-4	3.3 (0.4)	6.9 (1.1)	4.4 (0.8)
v_{14}	χ^2	Phe-4	Phe-4	1.7 (0.2)	3.2 (0.4)	3.0 (0.4)
v_{15}	ϕ	Phe-4	Phe-4	8.9 (1.3)	19.6 (3.2)	6.3 (1.2)
v_{16}	ψ	Phe-4	Met-5	4.5 (0.3)	8.0 (0.9)	4.4 (0.6)
v_{17}	ω	Phe-4	Met-5	1.8 (0.2)	8.1 (1.2)	5.4 (0.8)
v_{18}	χ^1	Met-5	Met-5	2.7 (0.2)	8.3 (2.5)	6.3 (1.9)
v_{19}	χ^2	Met-5	Met-5	1.9 (0.2)	5.3 (0.4)	4.0 (0.5)
v_{20}	χ^3	Met-5	Met-5	1.1 (0.1)	2.7 (0.2)	2.5 (0.2)
v_{21}	χ^4	Met-5	Met-5	1.0 (0.1)	1.3 (0.1)	1.3 (0.1)
v_{22}	ϕ	Met-5	Met-5	36 (18)	23.8 (5.6)	9.5 (2.4)
v_{23}	ϕ	Met-5	Met-5	1.4 (0.2)	1.9 (0.1)	1.9 (0.1)
v_{24}	ω	Met-5	Met-5	1.0 (0.1)	3.4 (0.2)	3.1 (0.4)
v_0	E			9.0 (1.7)	19.4 (3.1)	6.6 (1.1)

B. Structure

For all our simulations we applied the method outlined in subsection II B to determine local energy minima and some results are summarized in Table IV: $E_{0.1}$ and $E_{0.9}$ are the lower and upper 10% quantiles of the energy and N_{conf} denotes the number of minima of the time series prepared for further minimization. The lowest energy found in this minimization process is denoted by E_{min} and N_{hits} is the number of times the lowest energy configuration was hit. While the absolute values of $E_{0.1}$ and $E_{0.9}$ vary considerably from set to set, the differences $E_{0.9} - E_{0.1}$ stay similar. The explanation is that the ASP sets differ by large additive constants to the energy.

Again, the results of the JRF and BM solvent models are erratic. The BM model is entirely frozen, $N_{\text{conf}} = 2$ at

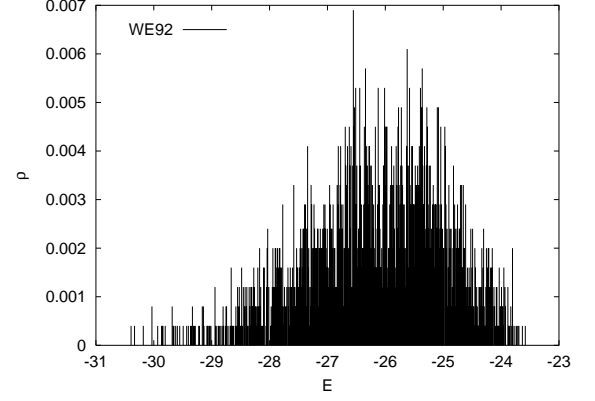


FIG. 5: Local energy minima for the WE92 solvation model as obtained by our minimization method.

400 K and $N_{\text{conf}} = 1$ at 300 K. Therefore, we do not give minimization results for BM. For JRF the N_{conf} numbers are more reasonable, but still by a factor of one third and less smaller than the N_{conf} numbers of each other system. JRF is also disregarded in the following discussion.

Only if $N_{\text{hits}} > 1$ holds we have an indication that we found the GEM. Interestingly, this happens for none of the ASP solvent models, while it is the case for the vacuum and the $\epsilon(r)$ simulations (notably already at 400 K). Quite some time ago Li and Scheraga [5, 11] developed a Monte Carlo minimization method and applied it to Met-Enkephalin in vacuum and in solvent modeled by OONS. While for the vacuum system their method converged consistently to the GEM, all their five runs of the solvent model led to different conformations with comparable energies. They interpreted their results in the sense that Met-Enkephalin in water at 20°C is likely in an unfolded state for which a large ensemble of distinct conformations co-exist in equilibrium. A consistent scenario was later observed in NMR experiments [33].

Although the minimization method of Li and Scheraga is entirely different from ours, they essentially tested for valleys of attraction to the GEM at room temperature, quite as we do in the present paper. So, we have not only confirmed their old result, but find that it is also common to a large set of ASP models implemented in SMMP. Neither the method by which an ASP set was derived, nor whether it belongs to the fast or slow class, appears to matter with this respect.

To give one example, the frequency of local energy minima of the WE92 solvation model as obtained by our minimization procedure from the 300 K time series is depicted in Fig. 5. $N_{\text{conf}} = 2453$ minimizations are performed. Our lowest energy state is only found once and the same holds for the close-by low energy states. Fig. 5 should be compared with Fig. 2 of Ref. [10], where the frequency of the low energy minima of the vacuum simulation is shown. There the lowest energy state relies on 107 entries out of 1913 minimizations [34].

TABLE IV: Determination of local minima: $E_{0.1}$ and $E_{0.9}$ are the lower and upper 10% quantiles of the energies of the time series recorded, N_{conf} denotes the number of configurations prepared for further minimization, E_{min} (Kcal/mol) is the lowest energy found, and N_{hits} is the number of times the lowest energy configuration was hit.

Set	$T = 400 \text{ K}$					$T = 300 \text{ K}$				
	N_{conf}	$E_{0.1}$	$E_{0.9}$	E_{min}	N_{hits}	N_{conf}	$E_{0.1}$	$E_{0.9}$	E_{min}	N_{hits}
VAC	2190	1.98	12.26	-12.91	13	1073	-2.98	5.73	-12.91	55
$\epsilon(r)$	2622	-16.95	-6.97	-31.94	8	1312	-21.85	-13.17	-31.94	27
OONS	3315	-17.83	-9.63	-27.69	1	2641	-21.40	-13.96	-28.93	1
JRF	448	-317.96	-304.98	-328.72	1	365	-323.66	-314.24	-332.87	1
WE92	3307	-19.88	-11.52	-29.44	1	2453	-23.43	-15.95	-30.39	1
EM86	2307	8.57	18.59	-4.11	1	1191	3.83	12.39	-5.47	1
SCH1	2511	5.57	15.45	-5.54	1	1147	0.71	9.33	-7.52	1
SCH2	3454	-22.17	-14.34	-31.32	1	2918	-25.31	-18.32	-32.71	1
SCH3	2315	8.57	18.32	-1.70	1	1229	4.29	12.50	-3.29	1
SCH4	2331	8.45	18.50	-4.93	1	1108	3.66	12.23	-5.16	1
BM	2	606.37	655.16	594.78	1	1	598.37	646.35	590.32	1

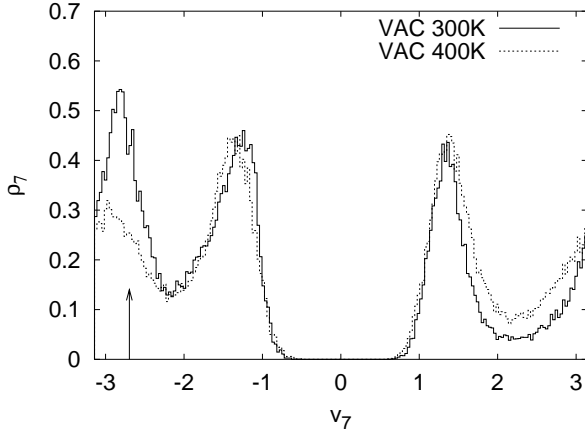


FIG. 6: Probability density of the dihedral angle v_7 for the vacuum simulation. The arrow indicates the vacuum GEM value of this angle.

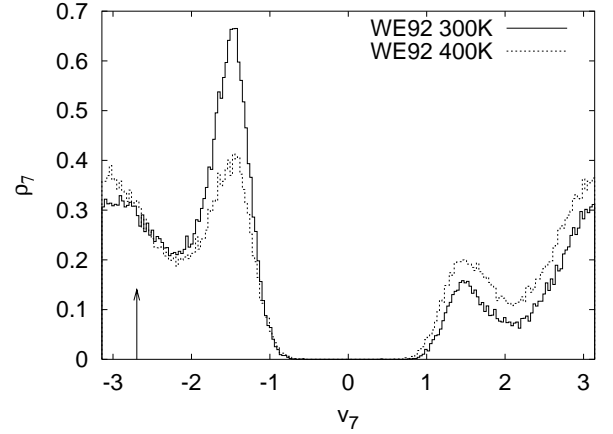


FIG. 7: Probability density of the dihedral angle v_7 for the WE92 simulation. The arrow indicates the vacuum GEM value of this angle.

In a search for structural differences of Met-Enkephalin in vacuum, or in the $\epsilon(r)$ system, versus the ASP models, we looked at the pds of the dihedral angles at 300 K. For all systems together there are $9 \times 24 = 216$ figures to consider. At the first look the pds of the different systems are amazingly similar, independently of whether they are from systems of the fast or slow class, from an ASP model, from the vacuum or from the $\epsilon(r)$ simulation. A more careful investigation reveals differences, which appear to relate to the distinct behavior under our minimization. For the dihedral angle v_7 this is illustrated in Fig. 6 and Fig. 7. Its probability densities are compared at 300 K and 400 K. For the vacuum simulation the pds are depicted in Fig. 6 and from 400 K to 300 K we observe an increase of the peak which is located close to the arrow, which indicates the vacuum GEM value of v_7 .

In contrast to this, the wrong peak increases in Fig. 7, where the pds are shown for the WE92 solvent model.

One may suspect that the difference between the models of our fast and slow class is simply due to an effectively higher temperature for the three models of the fast class. To gain insight into this question, we calculate the entropies of our pds. Each pd is discretized as a histogram of 200 entries, ρ_{ij} , where $i = 1, \dots, 24$ labels the dihedral angles according to Table III and $\sum_{j=1}^{200} \rho_{ij} = 1$. The entropy of the pd of a dihedral is then defined by

$$S_i = - \sum_{j=1}^{200} \rho_{ij} \ln \rho_{ij} \quad (10)$$

and the total entropy of the pds of an APS model is $S = \sum_i S_i$. In Fig. 8 the thus obtained entropies are

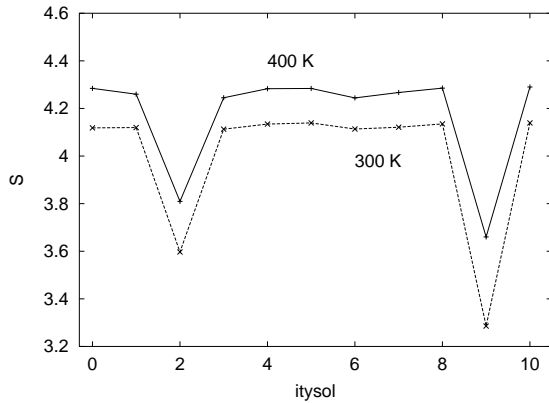


FIG. 8: Entropies of the pds of our ASP models. The models are labeled according Table I, in addition `itysol` = 0 for vacuum and `itysol` = 10 for the $\epsilon(r)$ model.

depicted for all our models. The lines between the data points have no other meaning but to guide the eyes. The dips for the JRF and the BM model show, again, that their configurations are essentially frozen. For the other we see a decrease of entropy from 400 K to 300 K, but we find no larger entropy for the models of the fast class than for the models of the slow class. Therefore, the effective temperature scenario is ruled out. Instead, it seems that for the models of the fast class the solvent has some kind of “lubrication” effect, which accelerates the simulation.

Strong similarities between the ASP models of the fast class on one side and the ASP models of the slow class on the other side are found for the solvation energies, the gyration radii and the end to end distances.

The solvation energies E_{sol} (3) measured during our simulations of ASP models are solvent-vacuum (s/v) transfer energies. There are structural difference between the typical configurations of an ASP model time series and the vacuum time series. Consequently, the average s/v transfer energies are not identical with the average vacuum-solvent (v/s) transfer energies, which are obtained by calculating E_{sol} of the solvent models on the configurations of the vacuum time series. The s/v as well as the -v/s average transfer energies are collected in Table V. The averages are taken for the canonical time series at 300 K and at 400 K. At 300 K averages are also taken for the time series minima (indicated by arrows in Fig. 1) and for the local minima (which are obtained by running the conjugate gradient minimizer on the time series minima). For the gyration radii R_{gy} and the end to end distances $R_{\text{e-e}}$ the same averages are collected in Table VI (definitions and software are given in SMMP).

For the transfer energies the over-all effect is hydrophilic for the APS models of the fast class and hydrophobic for the APS models of the slow class. Within each class the values are quite similar, despite differences in the interaction coefficients (see Table 1 of Ref.[13]). As expected the over-all transfer energies of the JRF and

BM models are out of the reasonable range, JRF to the hydrophilic and BM to the hydrophobic side. Our Table VI shows that we observe the extended structures found in previous simulations [11, 12] and in NMR experiments [33] only for the APS models of the fast class.

IV. SUMMARY AND CONCLUSIONS

We have performed Met-Enkephalin simulations at room temperature (300 K) for the solvation models of Table I. Quantitative results obtained in that way cannot be trusted, apparently because the methods to derive the ASPs have been quite crude. Also our simulations do not give information that would allow us to pick a best ASP set for the intended purpose of simulating Met-Enkephalin at 300 K. Nevertheless, we obtain a qualitative overview of a number of interesting consequences, which one can expect by including solvation effects via an ASP model in Metropolis calculations.

Two of the ASP sets (JRF [20] and BM [23] as implemented in SMMP [13]) suffer from so large autocorrelations that for them Metropolis simulations at 300 K are in essence impossible. Their dihedral angles are essentially frozen. These two ASP sets are certainly erratic, as 300 K is a temperature at which thermodynamic fluctuations of the systems are expected (also these two sets perform badly at 400 K).

The remaining nine models, seven ASP sets, $\epsilon = 2$ vacuum, and an $\epsilon(r)$ system [25], fall into a fast and a slow class with respect to their integrated autocorrelation times, see Fig. 4. Vacuum simulations are in the slow class. This leads to the interesting feature that it takes less computer time to estimate physical observables at room temperature in the fast solvation models OONS [17], WE92 [21], and SCH2 [19, 22], than it takes for vacuum, despite the substantial increase of the computer time per sweep by a factor of about 5 for the solvation models over the vacuum system. We have no clear clue why some models have a fast and others a slow dynamics. To derive the parameters of OONS and WE92 vacuum-water (v/w) transfer energies were used, but for SCH2 it was octanol-water (o/w). Also the slow class features v/w as well as o/w ASP models.

We applied the minimization procedure of Ref. [10] in an attempt to locate the GEM for the nine systems, which are reasonably well-behaved under Metropolis simulations at 300 K. The GEM is unambiguously found for the vacuum system and for the simulation with a distance dependent electrostatic permittivity. No true GEM is found for any of the remaining seven ASP models. This confirms an old result of Li and Scheraga [11], who concluded that at room temperature Met-Enkephalin in water is likely in an unfolded state. To get a better understanding of this result, we studied at 300 K the dihedral pds in some details. At a first glance they look quite similar for all the models in the fast as well as in the slow class. Differences are found for a number of details,

TABLE V: Transfer energies.

Set	$T = 300$ K						$T = 400$ K	
	$\langle E^T \rangle$ (Local min.)		$\langle E^T \rangle$ (Time series min.)		$\langle E^T \rangle$		$\langle E^T \rangle$	
	s/v	-v/s	s/v	-v/s	s/v	-v/s	s/v	-s/v
OONS	-24.85	-18.71	-24.63	-18.53	-24.84	-19.07	-24.94	-20.19
JRF	-346.95	-185.65	-346.72	-187.30	-343.56	-196.96	-337.68	-209.46
WE92	-28.84	-17.46	-28.52	-17.62	-27.87	-18.76	-27.47	-20.61
EM86	6.19	6.93	6.29	7.01	6.45	7.08	6.60	7.11
SCH1	2.76	3.89	2.86	3.92	2.94	3.80	2.97	3.60
SCH2	-31.03	-20.61	-30.77	-20.80	-30.61	-21.97	-30.45	-23.85
SCH3	4.03	9.73	4.28	9.80	4.74	9.50	5.15	9.00
SCH4	6.08	6.86	6.17	6.93	6.32	6.95	6.46	6.94
BM	—	715.29	=	721.43	581.60	745.22	597.61	776.03

TABLE VI: Gyration radii and end to end distance.

Set	$T = 300$ K						$T = 400$ K	
	Local minima		Time series minima		Time series		Time series	
	$\langle R_{gy} \rangle$	$\langle R_{e-e} \rangle$	$\langle R_{gy} \rangle$	$\langle R_{e-e} \rangle$	$\langle R_{gy} \rangle$	$\langle R_{e-e} \rangle$	$\langle R_{gy} \rangle$	$\langle R_{e-e} \rangle$
VAC	4.56	5.67	4.60	5.83	4.72	6.83	4.97	8.50
ϵr	4.53	6.20	4.57	6.33	4.71	7.39	4.99	8.94
OONS	4.92	10.30	4.94	10.34	5.32	11.71	5.60	12.45
JRF	5.75	13.00	5.75	13.00	5.78	13.05	5.70	13.20
WE92	5.06	12.06	5.07	12.09	5.43	13.02	5.72	13.47
EM86	4.47	6.97	4.48	7.02	4.62	7.94	4.86	9.28
SCH1	4.51	6.96	4.52	7.02	4.68	7.96	4.96	9.45
SCH2	5.18	12.48	5.20	12.53	5.63	13.47	5.86	13.66
SCH3	4.54	8.88	4.55	8.90	4.72	9.56	4.95	10.50
SCH4	4.46	6.82	4.47	6.87	4.62	7.83	4.87	9.17
BM	—	—	—	—	4.13	7.30	4.21	7.66

which may allow to explain why the 300 K configurations of the ASP models behave entirely different under our minimization procedure than the vacuum and the $\epsilon(r)$ systems.

The central question, which remains to be settled, is whether ASP models will ultimately allow for accurate Metropolis simulations of biomolecules like Met-Enkephalin in solvent or not. In principle, this could be decided by determining whether ASPs exist which reproduce accurately mean energies of explicit solvent simulation around a large number of fixed Met-Enkephalin configurations.

Acknowledgments

We would like to thank Prof. P. Grassberger for useful discussions and generous support of this work. The computer simulations were carried out on the Cray T3E of the John von Neumann Institute for Computing. BB acknowledges partial support by the U.S. Department of Energy under contract No. DE-FG02-97ER41022. In the final stage of this work we became aware of two articles where ASP models are studied for the helix-coil transition of polyalanine [35].

-
- [1] B. Lee and M. Richards, J. Mol. Biol. **55**, 379 (1971).
 - [2] C. Cothia, Nature **248**, 338 (1974).
 - [3] D. Eisenberg, A.D. McLachlan, Nature **319**, 199 (1986).
 - [4] A.H. Juffer, F. Eisenhaber, S.J. Hubbard, D. Walther, P. Argos, Protein Sci. **4**, 2499 (1995).
 - [5] Z. Li and H.A. Scheraga, Proc. Nat. Acad. Sci. USA, **85**,

- 6611 (1987).
- [6] Y. Okamoto, T. Kikuchi, and H. Kawai, Chem. Lett. **1992**, 1275 (1992).
- [7] U.H. Hansmann and Y. Okamoto, J. Comp. Chem. **14**, 1333 (1993).
- [8] H. Meirovitch, E. Meirovitch, A.G. Michel, and M.

- Vásquez, J. Phys. Chem. **98**, 6241 (1994).
- [9] U.H. Hansmann, Y. Okamoto, and J.N. Onuchic, PROTEINS: Structure, Function, and Genetics **34**, 472 (1999).
 - [10] B.A. Berg Phys. Rev. Lett. **90**, 180601 (2003).
 - [11] Z. Li and H.A. Scheraga, J. Mol. Struct. (Theochem) **179**, 333 (1988).
 - [12] M. Kinoshita, Y. Okamoto, and F. Hirata, J. Am. Chem. Soc. **120**, 1855–1863 (1998).
 - [13] F. Eisenmenger, U.H. Hansmann, S. Hayryan, and C.-K. Hu, Comp. Phys. Commun. **138**, 192 (2001).
 - [14] G.J. Geyer, in *Computing Science and Statistics*, Proceedings of the 23rd Symposium on the Interface, E.M. Keramidis (editor), Interface Foundation, Fairfax, Virginia, 1991, pp.156–163.
 - [15] K. Hukusima and K. Nemoto, J. Phys. Soc. Japan **65**, 1604 (1996).
 - [16] U.H. Hansmann, Chem. Phys. Lett. **281** 140 (1997).
 - [17] T. Ooi, M. Obatake, G. Nemethy, and H.A. Scheraga, Proc. Natl. Acad. Sci. USA **84**, 3086 (1987).
 - [18] D. Eisenberg, M. Wesson, M. Yamashita, Chem. Scrip. **A 29**, 217 (1989).
 - [19] A. Kim, *Amino acid side chain contributions to free energy of transfer of tripeptides from water to octanol*, dissertation, University of California at San Francisco, 1990.
 - [20] J. Vila, R. L. Williams, M. Vásquez, H. A. Scheraga, Proteins Struct. Funct. Genet. **10** 199 (1991).
 - [21] L Wesson, D. Eisenberg, Protein Sci, **1**, 227 (1992).
 - [22] C. A. Schiffer, J. W. Caldwell, P.A. Kollman, and R. M. Stroud, Mol. Simul. **10**, 121 (1993).
 - [23] B. von Freyberg, T. J. Richmond, and W. Braun, J. Mol. Biol. **233**, 275 (1993).
 - [24] M.J. Sippl, G. Nemethy, and H.A. Scheraga, J. Phys. Chem. **88**, 6231 (1984) and references given therein.
 - [25] B. Hingerty, R.H. Richie, T.L. Ferrel, and J. Turner, Biopolymers **25**, 427 (1985).
 - [26] Y. Okamoto, Biopolymers **34**, 529 (1994).
 - [27] J.L. Fauchere and V. Pliska, Eur. J. Med. Chem. Chim. Ther. **18**, 369 (1983).
 - [28] S. Cabani, P. Gianni, V. Mollica, and L. Lepori, J. Solution Chem. **10**, 563 (1981).
 - [29] R. Wolfenden, L. Andersson, P.M. Cullis, and C.C.B. Southgate, Biochemistry **20**, 849 (1981).
 - [30] S. Brandt, *Statistical and Computational Methods in Data Analysis* (North-Holland Publishing Company, Amsterdam, 1983).
 - [31] A. Sokal, in *Functional Integration: Basics and Applications*, C. DeWitt-Morette, P. Cartier and A. Folacci (editors), Cargese Summer School, Plenum Press, New York, 1997, pp.131–192.
 - [32] M. Masuya and Y. Okamoto, quoted in Y. Okamoto, Rec. Res. Dev. in Pure & Appl. Chem. **2**, 1 (1998).
 - [33] W.H. Graham, E.S. Carter II, and R.P. Hicks, Biopolymers **32**, 1755 (1992).
 - [34] By mistake 1357 instead of 1913 was reported in [10].
 - [35] Y. Peng, U.H. Hansmann, and N.A. Alves, J. Chem. Phys. **118**, 2374 (2003); Y. Peng and U.H. Hansmann, Biophys. J. **82**, 3269 (2003).